Behavior of Glass Fiber Reinforced Polymer Concrete Panels

Hussain Fadhil Hussain
Department of Water Resources Engineering, College of Engineering, University of Baghdad, Baghdad, Iraq
hussain.fadhel@coeng.uobaghdad.edu.iq

Alaa Hussein Al-Zuhairi
Department of Civil Engineering, College of Engineering, University of Baghdad, Baghdad, Iraq
alaalwn@coeng.uobaghdad.edu.iq

Zainab Kareem Al-Mamory
Department of Civil Engineering, College of Engineering, University of Baghdad, Baghdad, Iraq
z.abd1901m@coeng.uobaghdad.edu.iq

Ali Hussein Ali Al-Ahmed
Department of Civil Engineering, College of Engineering, University of Baghdad, Baghdad, Iraq
dr.ali-alahmed@coeng.uobaghdad.edu.iq (corresponding author)

Received: 25 September 2024 | Revised: 20 November 2024 | Accepted: 28 November 2024

 DOI: https://doi.org/10.48084/etasr.9100

ABSTRACT

Glass Fiber Reinforced Polymer (GFRP) bars have gained popularity as a corrosion-resistant alternative to traditional steel reinforcement in Reinforced Concrete (RC) elements. This study investigates the flexural behavior of PRC panels reinforced with GFRP bars. The study variables included the GFRP reinforcement ratio and the number of embedded steel section distributions. Six concrete panels were fabricated, each measuring 2500 mm in length, with a rectangular cross-section of 750 mm in width and 150 mm in thickness. All panels were reinforced with GFRP bars and divided into two groups based on the reinforcement ratios of 0.532% and 0.266%. For each group, one panel served as the control specimen, while the remaining two were internally strengthened with embedded steel box sections, one with 2 steel sections and the other with 4 sections. The parametric study highlighted the effects of the reinforcement ratio and the inclusion of internal I-section steel shapes on the flexural performance of the panels. Compared to non-strengthened control slabs, the addition of steel elements significantly improved the structural performance, as evidenced by reductions in deflection, strains, and crack widths, as well as an increase in the ultimate load capacity and flexural stiffness at the ultimate loading stage. These findings underscore the effectiveness of combining GFRP reinforcement with embedded steel shapes to enhance the structural performance of PRC panel slabs.

Keywords- GFRP; steel box section; precast panel

I. INTRODUCTION

The Precast Concrete (PC) methodology has emerged as an effective approach to drive innovation and modernization in the construction industry. This methodology is cost-efficient, environmentally friendly, and contributes to reducing the carbon emissions. The PC technology enhances efficiency and quality control during the manufacturing of concrete elements, significantly reducing the need for formwork and wet work in on-site casting while minimizing construction-related pollution [1]. Fiber-Reinforced Polymer (FRP) materials are manufactured in a wide range of shapes and are extensively employed in concrete structures both as reinforcement and as strengthening solutions [2-4]. In harsh environmental conditions, steel reinforcement is susceptible to rapid corrosion, leading to costly repair and maintenance, reduced structural service life, and, in extreme cases, structural failure due to the corrosion of steel rebar [5-7].

Various types and sizes of FRP reinforcing bars are now available, including Carbon Fiber-Reinforced Polymer (CFRP) bars [9], Aramid Fiber-Reinforced Polymer (AFRP) bars, Glass Fiber-Reinforced Polymer (GFRP) bars, and others [8, 10]. GFRP bars have been developed as a non-corrosive alternative

to steel reinforcement for diverse structural concrete applications. They are particularly well-suited for aggressive environments, where steel reinforcement is prone to corrosion [11-13]. Over the last decade, the adoption of GFRP bars has grown due to their lightweight nature, ease of handling and installation, anti-corrosive properties, cost-effectiveness (relative to other FRP types), and high tensile strength [14-16]. Concrete structural elements, particularly RC panels reinforced with FRP bars, tend to exhibit lower stiffness and greater deformation compared to those reinforced with steel rebars. To address this limitation, various techniques have been developed to enhance the stiffness of RC panels, including external strengthening with steel sections and external prestressing with steel strands [17]. However, these methods often increase the sectional depth of the panels, which can conflict with architectural, plumbing, and mechanical design requirements [18]. Consequently, an alternative approach is needed to overcome these challenges [19, 20]. One potential solution is the incorporation of embedded steel sections to enhance the stiffness of GFRP-PC panels.

The effectiveness of steel-based strengthening largely depends on the allowable stress levels. Two options exist: reinforcing elements within their elastic range or permitting partial yielding. Maintaining reinforcement in the elastic range means that the strengthening element only bears loads applied after its installation, which is an inefficient solution. In contrast, the plastic analysis allows stress redistribution and full utilization of the newly incorporated material. Under plastic conditions, the stress level in the reinforced element does not constrain the ultimate load capacity of the section [21]. Despite advancements, there is limited research on upgrading GFRP-concrete panels with internally embedded steel sections. This study investigates concrete panels reinforced with GFRP bars at two different reinforcement ratios and internally strengthened with steel box sections of varying sizes along their span.

II. EXPERIMENTAL WORK

The experimental program involved testing six one-way concrete panel slabs reinforced with GFRP bars. All slabs were prismatic, with rectangular cross-sections measuring 2500 mm in length, 750 mm in width, and 150 mm in thickness. The test specimens were divided into two groups based on the GFRP reinforcement ratio, as shown in Table I.

TABLE I. DESING OF THE EXPERIMENTAL TEST PANELS

Group	Panel design	Characteristic	Dimensions of steel box (mm)	No. of steel sections	GFRP reinforcement ratio
Group 1	CP-1	(control)	-	-	0.00532
	P-1-2S	Concrete panel with two embedded steel box sections	50 × 80 × 4.8	2	0.00532
	P-1-4S	Concrete panel with four embedded steel box sections	30 × 50 × 4	4	0.00532
Group 2	CP-2	(control)	-	-	0.00266
	P-2-2S	Concrete panel with two embedded steel box sections	50 × 80 × 4.8	2	0.00266
	P-2-4S	Concrete panel with four embedded steel box sections	30 × 50 x 4	4	0.00266

The first group comprised three panels reinforced with 10ϕ8 mm GFRP bars (ρ = 0.00532). One specimen in this group was designated as the reference panel, while the other two were fabricated with embedded steel box sections for additional strengthening. The first strengthened specimen incorporated two hollow steel boxes with cross-sectional dimensions of 50 mm × 80 mm and a wall thickness of 4.8 mm. These steel sections were distributed across the panel's width.

The second strengthened specimen included four hollow steel boxes, each with cross-sectional dimensions of 30 mm × 50 mm and a wall thickness of 4 mm, also distributed across the width, as illustrated in Figure 1. Notably, the total cross-sectional area of the hollow steel sections was approximately equal for both strengthened specimens. Specifically, the area of a steel box with dimensions 50 mm × 80 mm × 4.8 mm was double that of a steel box with dimensions 30 mm × 50 mm × 4 mm. The second group also consisted of three panels, but these were reinforced with 5ϕ8 mm GFRP bars (ρ = 0.00266). The distribution of specimens within this group followed the same pattern as the first group, as depicted in Figure 2.

A. Material Properties

1) Concrete

The slab specimens were fabricated using Self-Compacting Concrete (SCC) with a cylinder compressive strength of approximately 40 MPa. The concrete mix comprised ordinary Portland cement (Type I), natural sand, crushed coarse aggregate with a maximum size of 10 mm, silica fume, stone powder, third-generation superplasticizer, and water. To determine the average compressive strength of the concrete, a total of six test samples were prepared: six standard cubes measuring 150 × 150 × 150 mm and six standard cylinders measuring 300 × 150 mm. The concrete mixture was consisted of cement (400 kg/m^3), sand (840 kg/m^3), gravel (1000 kg/m^3), water (180 L/m^3), and the Water-to Cement (*W/C*) ratio (0.45).

2) GFRP Bars

All concrete slabs were reinforced with 8 mm diameter deformed GFRP bars to enhance durability. According to the manufacturer's specifications, the mechanical properties of the GFRP bars are as follows: ultimate tensile strength of about 900 MPa, modulus of elasticity of 40 GPa, weight of 77.4 g/m, and transverse shear strength of 150 MPa.

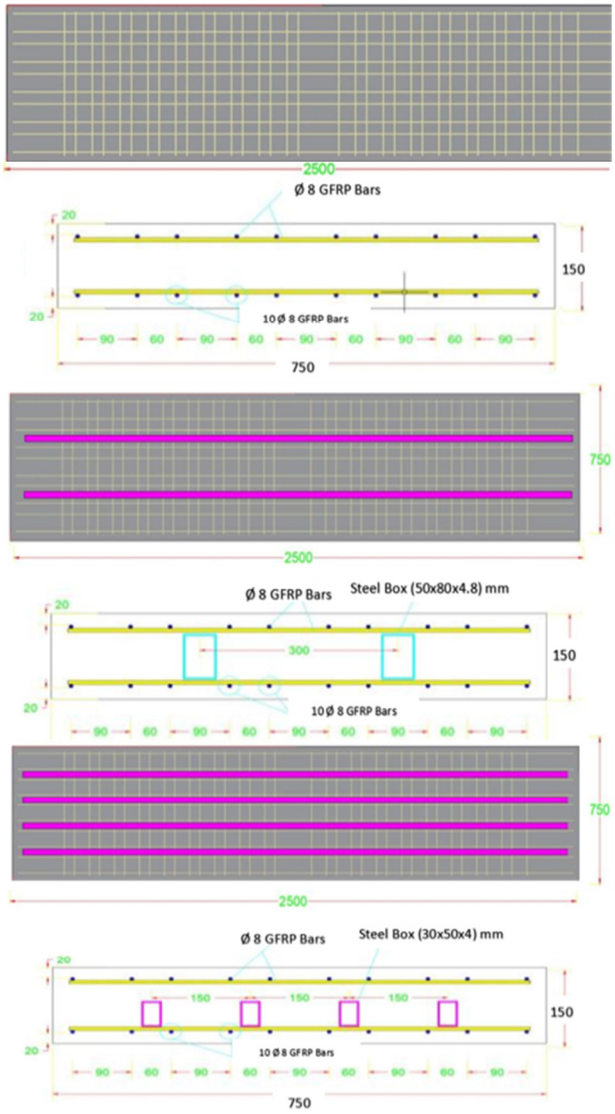

Fig. 1. Characteristics of the 1st group of the experimenal panels.

3) *Steel box-shapes*

Hot rolled steel box sections were utilized in two different sizes and encased longitudinally within the specimens. The two hollow box section dimensions were: 30 × 50 × 4 mm and 50 × 80 × 4.8 mm. To determine the mechanical properties of these sections, multiple coupons were extracted and tested. The test results revealed the following average values: yield stress of approximately 340 MPa and the ultimate strength of about 480 MPa.

B. *Preparation of the Test Panels*

The fabrication of each test panel began with the preparation of the GFRP bars. Standard 8 mm diameter GFRP bars, originally supplied in 6 m lengths, were cut to the required lengths of 250 cm for longitudinal reinforcement and 75 cm for transverse reinforcement using an electric rebar cutter. The cut GFRP bars were assembled to form the reinforcement cage, which was secured using thin steel wires. Steel box sections were then fixed at the bottom of the reinforcing mesh, as illustrated in Figure 3.

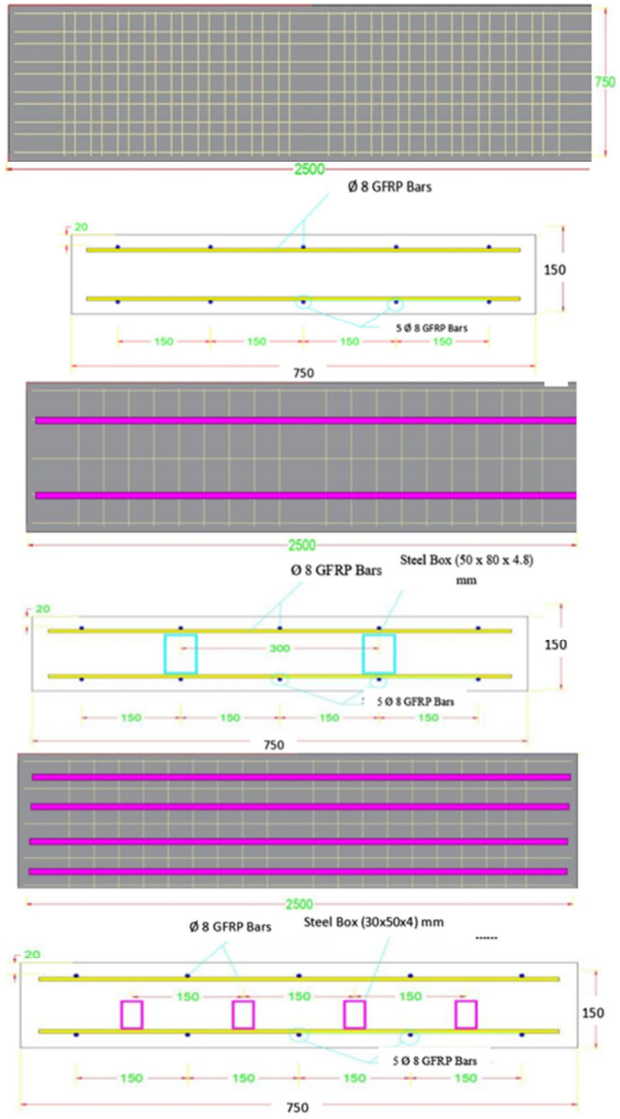

Fig. 2. Characteristics of the 2nd group of the experimenal panels.

C. *Test Instrumentation and Measurements*

In this experiment, the panels were simply supported on two steel beams spaced 2400 mm apart, 28 days after casting. A hydraulic jack, with a load capacity of 500 kN, was used to apply the load. Each slab was subjected to a four-point bending test, loaded monotonically until failure, as displayed in Figure 4. To measure deflection, two Linear Variable Differential Transducers (LVDTs) and one dial gauge were used. These instruments were positioned at the midpoint of each slab and were attached to a supplementary steel frame for stability. Additionally, two strain gauges were installed at the center of one of the middle longitudinal reinforcing bars, and one strain gauge was placed at the center of a steel box. The strain gauges were positioned at the bottom of the GFRP bar reinforcement and the bottom of the steel box, as shown in Figure 5.

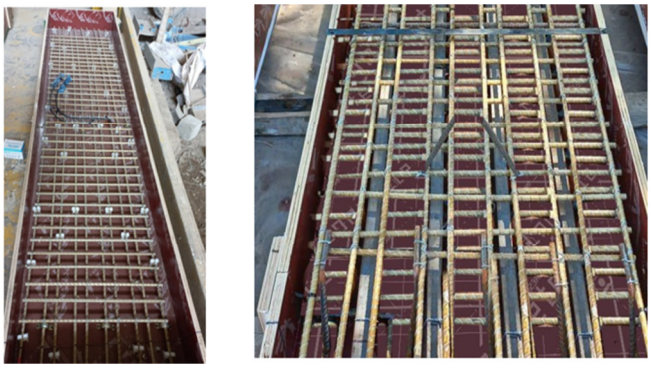

Fig. 3. Illustration of the experimental panels.

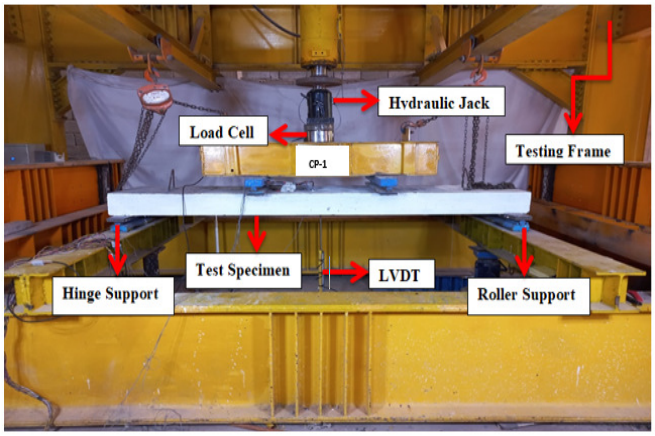

Fig. 4. Setup of a typical test panel.

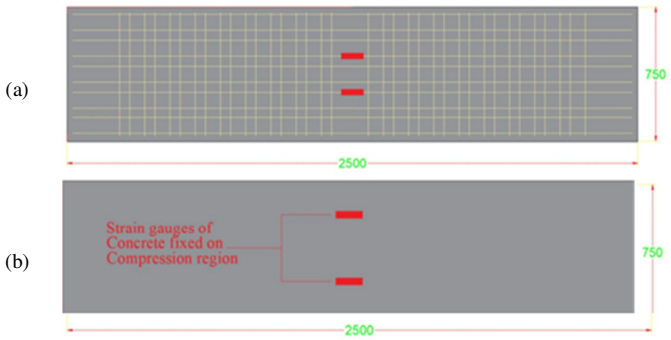

Fig. 5. Position of the GFRP strain gauge: (a) bottom reinforcement mesh and (b) top face of specimens.

To measure the concrete compressive strain, two strain gauges, each with a gauge length of 60 mm, were affixed to the concrete compression area of all slab specimens. These gauges were positioned at the midpoint of the top surface of the slabs, located at mid-span.

III. RESULTS

This study evaluates the behavior of GFRP-RC panel slabs. To facilitate the comparisons between solid and strengthened panels and to provide a deeper understanding of their performance, Table II presents the key parameters, which are necessary for this analysis. These parameters include: the first cracking load (P_{cr}), mid-span deflection at ultimate load (Δ_u), ultimate load (P_u), as well as the type and mode of failure.

TABLE II. KEY PARAMETERS FOR ALL TESTED SPECIMENS

Group	Slab design	P_{cr} (kN)	Δ_u (mm)	P_u (kN)	Type of failure	Failure mode
Group 1	CP-1	35	88	130	Flexural tensile failure	Brittle (GFRP-rupture)
	P-1-2S	38	74	310	Flexural compression failure	Brittle (GFRP-rupture)
	P-1-4S	42	71	323	Flexural compression failure	Brittle (concrete - crushing)
Group 2	CP-2	22	98	111	Flexural tensile failure	Brittle (Concrete crushing)
	P-2-2S	24	83	276	Flexural compression failure	-
	P-2-4S	25	82	289	Flexural compression failure	-

A. Load Deflection Response

All six panels, as summarized in Table II, exhibited a flexural mode of failure. The load versus mid-span deflection curves for the test panels are portrayed in Figure 6.

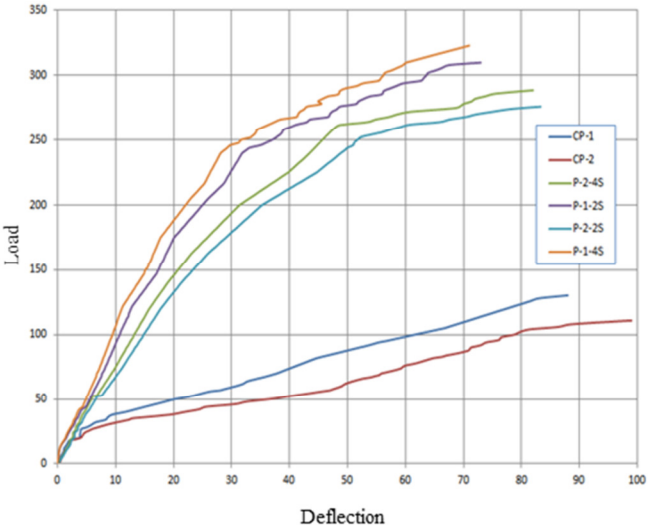

Fig. 6. Load versus mid span deflection of all test panels.

During the initial loading phase, no cracks were observed in any of the panels, resulting in a linear load-deflection response. This behavior can be attributed to the linear elastic properties of both the concrete and GFRP bars. Once the concrete cracked, a significant reduction in flexural stiffness was observed. As the load increased, additional cracks formed along the span of the panels, further reducing their flexural stiffness. The control panels (without embedded steel boxes) displayed greater deflection compared to the strengthened

panels. Generally, the inclusion of embedded steel boxes improved the flexural performance of the panels, resulting in a notable increase in both stiffness and ultimate load capacity. From the load-deflection curves, it is evident that the panels strengthened with four steel boxes demonstrated higher stiffness and ultimate load capacity compared to those with two steel boxes. This improvement can be attributed to the distributed placement of the total steel area across the panel cross-section within the tension zone, which provided additional reinforcement to the GFRP bars.

B. Crack Pattern and Mode of Failure

Figure 7 illustrates the crack patterns observed in the test panel slabs.

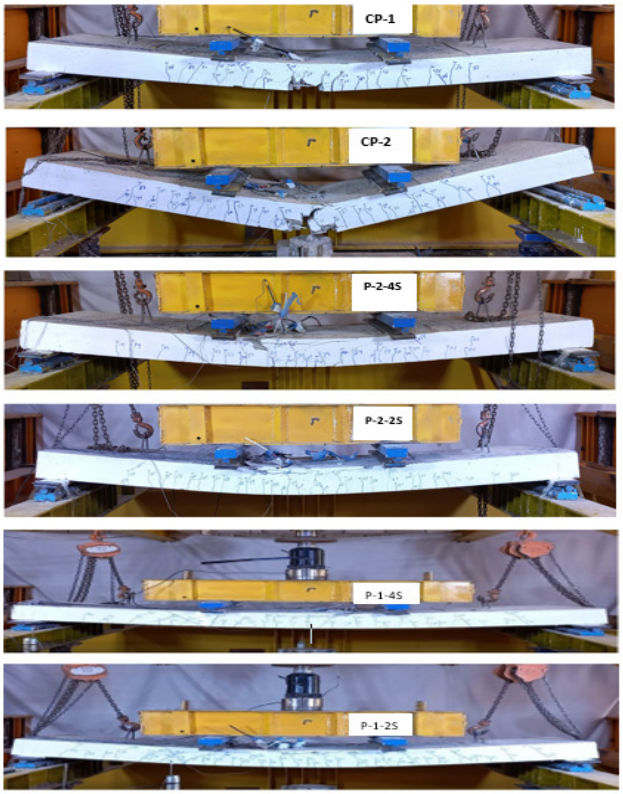

Fig. 7. Failure mode and crack pattern of all tested specimens.

The behavior of the control panels (CP-1 and CP-2) under loading can be summarized as follows:

- Crack Initiation: Flexural cracks initially formed in the flexural zone during the early stages of loading.
- Crack Extent: As the load increased, additional cracks appeared and spread along the span of the panel.
- Deflection Increase: With continued loading, mid-span deflection increased rapidly, accompanied by the widening of the existing cracks.
- Failure Mode: Cracks propagated toward the compression face of the specimens, leading to the strain in the GFRP bars reaching their ultimate limit, resulting in rupture. The mode of failure for these specimens was identified as flexural tensile failure.

For panels strengthened with embedded steel boxes, the behavior differed significantly:

- Crack Formation: Flexural cracks were observed following the formation of the first crack.
- Crack Development: Additional cracks developed and spread along the span but exhibited narrower widths compared to the control panels. These cracks also propagated toward the compression face.
- GFPR Strains: The strains in the GFRP bars remained within the elastic range, and no rupture of the bars was observed.
- Failure Mode: All strengthened panels exhibited flexural failure without GFRP rupture.

C. Load-Concrete Compressive Strain Response

1) Concrete Strain

The compressive behavior of the concrete was analyzed using the average measurements from two strain gauges placed in the compression zone at the center of the upper face of each specimen. Prior to crack formation and concrete crushing, the strain gauge readings were negligible. Once cracks were initiated, the strain steadily increased as the applied load increased, ultimately leading to failure, as exhibited in Figure 8.

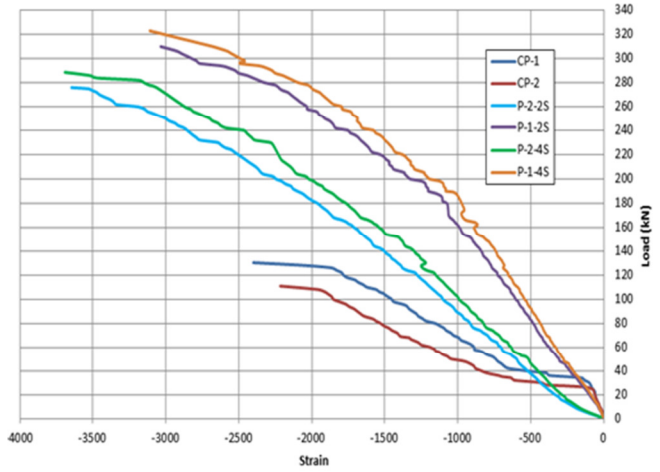

Fig. 8. Load versus compressive strain of concrete of all tested specimens.

To facilitate a comparative analysis, the service load of the solid slabs (CP-1 and CP-2), defined as 0.85 P_u [22], was used as a reference point to limit the deviations in strain for each slab. For the first group, Figure 9 demonstrates that the strengthened slabs (P-1-2S) and (P-1-4S) exhibited higher strain levels compared to the unstrengthened slab (CP-1) at the same load level. Specifically, the strain of specimens P-1-2S and P-1-4S was 26% and 29 %, respectively higher than that of specimen CP-1. This increase in strain for the strengthened specimens is attributed to the reduced stiffness of CP-1, relative

to the strengthened slabs. The presence of embedded steel boxes, combined with the reduced concrete volume, led to increased flexibility in the strengthened slabs. For the second group, the slabs strengthened with a decreased reinforcement ratio (P-2-2S and P-2-4S) exhibited higher strain levels than the slabs with a higher reinforcement ratio. This increase in strain is attributed to the reduction in the reinforcement ratio, which decreased the stiffness of the specimens.

Table III summarizes the strain values for all specimens under identical loading conditions, including at the ultimate stage and the service load stage (0.85 P_u of CP-1 and CP-2), for both concrete and GFRP bars.

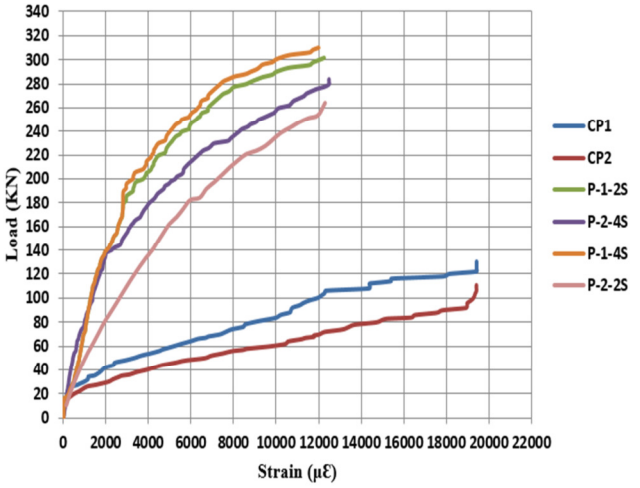

Fig. 9. Load versus strain of bottom GFRP bars.

TABLE III. STRAIN OF GFRP AND CONCRETE AT SERVICE AND ULTIMATE LOADING STAGE FOR ALL TESTED SPECIMENS.

Slab Design	P_u (kN)	Avg. Strain at the service load stage (0.85 P_u)		Avg. Strain at the ultimate loadiing stage (με)	
		GFRP bar (με)	Concrete (με)	GFRP-bar (με)	Concrete (με)
CP-1	130	14381.01	1622.94	19411.95	2400.87
P-1-2S	310	6418.58	2055.21	12251.24	3035.19
P-1-4S	323	6999.41	1986.04	11981.18	3110.32
CP-2	111	18987.33	1744.96	19422.17	2216.04
P-2-2S	276	9861.5	2789.46	12297.6	3645.80
P-2-4S	289	8656.30	2624.60	12480.50	3691.59

D. Flexural Stiffness of Slabs

Flexural stiffness describes a structural element's ability to resist deformation due to bending. It is influenced by the slab's elastic modulus, moment of inertia, effective length, and boundary conditions. The flexural stiffness of the slabs was evaluated using the secant stiffness method, determined by the load-deflection slope at specific loading stages. As load is applied, the stiffness of the slabs decreases progressively due to the development of cracks and insufficient bonding between the concrete and reinforcement bars. The secant stiffness was calculated using the following equations:

$$K_{cr} = \frac{P_{cr}}{\Delta_{cr}} \quad (1)$$

$$K_u = \frac{P_u}{\Delta_u} \quad (2)$$

where K_{cr} and K_u represent the stiffness at the flexural cracking stage and the ultimate stage, respectively.

Table IV presents the results of secant stiffness calculations for the cracking and ultimate stages. It is evident that the ultimate stiffness values (K_u) for all specimens are lower than their cracking stiffness values (K_{cr}). This reduction in stiffness can be attributed to voids within the slab and a subsequent decline in flexural rigidity during both the cracking and ultimate loading stages.

TABLE IV. STIFFNESS AT CRACKING AND ULTIMATE STAGE FOR ALL TESTED SPECIMENS.

Slab Design	Cracking Stage			Ultimate stage		
	P_{cr} (kN)	Δ_{cr} (mm)	K_{cr} (kN/mm)	P_u (kN)	Δ_u (mm)	K_u (kN/mm)
CP-1	35	8.29	4.22	130	88	1.48
P-1-2S	38	5.8	6.55	310	74	4.19
P-1-4S	42	3.7	11.35	323	71	4.55
CP-2	22	2.86	7.69	111	98	1.13
P-2-2S	24	2.97	8.08	276	83	3.33
P-2-4S	25	2.65	9.43	289	82	3.52

When considering the material and design characteristics used in the models, distinct variations were observed in the stiffness ratios of the specimens at both stages.

Second Group (Lower Reinforcement Ratio):

- For specimen P-2-2S, the flexural stiffness increased by approximately 5% at the cracking stage and 195% at the ultimate stage compared to the specimen CP-2.
- For specimen P-2-4S, there was an increase of about 22% at the cracking stage and 211% at the ultimate stage compared to specimen CP-2.
- These improvements are attributed to the strengthening effect of the embedded steel boxes, with greater increases for specimens with more steel boxes.

First Group (Higher Reinforcement Ratio):

- For specimen P-1-2S, the stiffness at the cracking stage improved by approximately 55%, while at the ultimate stage, the increase was around 183% compared to specimen CP1.
- For specimen P-1-4S, the stiffness improved by about 168% at the cracking stage and 207% at the ultimate stage compared to specimen CP1.
- The enhanced stiffness in these specimens is primarily due to the inclusion of embedded steel sections, which increased the moment of inertia and provided additional resistance to deformation.

IV. FINITE ELEMENT MODEL OF CONCRETE BEAMS

A 3D Finite Element Model (FEM) of the normal concrete slab specimen was developed using the nonlinear finite element software ABAQUS to predict the flexural behavior of the beam

specimen [23, 24]. The normal concrete was modeled in the FEM using the Concrete Damage Plasticity Model (CDPM) [25]. The required material behaviors, including stress-strain relationships, were directly input into the selected model.

A. Model Elements and Configuration

The concrete and supporting plate were modeled using three-dimensional, eight-nodded linear brick elements (C3D8R), which are hexahedral elements with reduced integration and hourglass control. Stirrups and GFRP rebars were represented utilizing two-nodded linear 3D truss elements (T3D2), while the steel box used for strengthening was modeled as a shell element with a specified thickness. The discretized slab elements for concrete and GFRP bars, as displayed in Figure 10, incorporated the CDPM to simulate the nonlinear behavior of normal concrete [26, 27]. This model required critical parameters, such as modulus of elasticity, Poisson's ratio, compressive and tensile stress-plastic strain behavior, and five plastic damage parameters, as detailed in Table V.

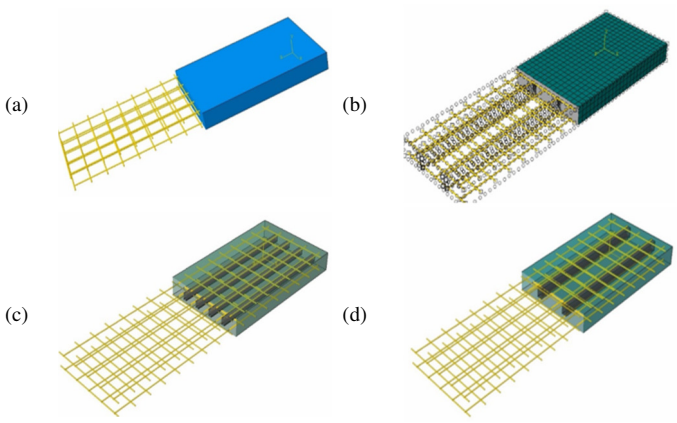

Fig. 10. Simulation of the specimens using the Abaqus program: (a) reinforcement concrete, (b) discretized slab elements for concrete and GFRP bars, (c) reinforcement concrete of four steel boxes, and (d) reinforcement concretr of two steel boxes.

TABLE V. CONCRETE DAMAGE PLASTICITY PARAMETERS AND GOVERN FORMULAS.

Parameter	Selected value
Material model	CDP model
E, MPa	27465.2
Poisson's ratio	0.2
Dilation angle, Ψ	30
Eccentricity of the flow potential, €	0.1
The ratio of biaxial to uniaxial strength, *fb0/fc0*	1.16
Rate of the tensile to the compressive meridian, *K*	0.667
Ωiscosity parameter, μ	0.0005

B. Concrete Behavior

The compressive behavior of concrete was modeled using a softening relationship derived from the theory proposed by Kratzig and Polling. This model is well-suited for numerical analysis as it depends on the mesh element length (l_{cq}). The compressive stress-strain relationship is given by:

$$\sigma_c^3 = \left(\frac{2+\gamma_c f_{com}\varepsilon_{c1}}{2f_{com}} - \gamma_c\varepsilon_c + \frac{\varepsilon_c^2\gamma_c}{2\varepsilon_{c1}}\right)^{-1} \quad (3)$$

$$e\gamma_c = \frac{\pi^2 f_{com}\varepsilon_{c1}}{2\left[\frac{G_{cb}}{l_{cq}} - 0.5 f_{cov}\left(\varepsilon_{c1}(1-\mathrm{b}) + b\frac{f_{cm}}{E_0}\right)\right]^2} \quad (4)$$

$$b = \frac{\varepsilon_c^{\beta l}}{\varepsilon_c^{in}} \quad (5)$$

where G_{cb} denotes the crushing energy, $\varepsilon_c^{\beta l}$ and ε_c^{in} are the plastic strain and inelastic strain, respectively.

The tensile behavior of concrete was represented using the stress-crack opening relationship proposed by Hordijk, which is independent of the mesh element size. This relationship is expressed as [27]:

$$\frac{\sigma_t(w)}{f_{twp}} = \left[1 + \left(c_1\frac{w}{w_t}\right)^3\right]e^{-c_2\frac{w}{w_t}} - \frac{w}{w_t}(1+c_1^3)e^{-c2} \quad (6)$$

where c_1 = 3, c_2 = 6.93, and w_t is the critical crack opening given by:

$$w_c = 5.14\frac{G_F}{f_{tm}} \quad (7)$$

Based on this stress-crack opening relationship, a stress-strain curve can be derived through:

$$\varepsilon_t = \varepsilon_{tm} + \frac{w}{l_{cq}} \quad (8)$$

where l_{cq} is the element length in the FEM mesh. Figure 11 illustrates this stress-strain relationship.

C. GFRP Bars Modeling

The GFRP bars were modeled in ABAQUS assuming isotropic, linear elastic behavior without any damage criteria [28-29]. The properties of the GFRP bars used in this study are presented in Table VI.

TABLE VI. MATERIAL CHARACTERISTICS USED IN FEM FOR GFRP BARS

Property	Value
Density	2100 kg/m^3
Young's modulus	70 GPa
Poisson's ratio	0.33
Failure stress	1400 MPa
Plastic strain	0.0002

D. Contact Interactions

Contact interactions in the FEM were defined to accurately simulate the interaction between different components of the slab system. The interface between the concrete and GFRP bars was modeled using an embedded contact approach, ensuring that the GFRP reinforcement behaves as an integral part of the concrete matrix. Surface-to-surface contact was utilized to represent the interaction between the bottom concrete slab and the supporting plates. This included normal behavior defined as "hard contact," which prevents penetration between surfaces under compression, and tangential behavior characterized by a penalty friction coefficient of 0.35 to account for sliding resistance [29, 30].

E. Load Application and Boundary Conditions

The static-general step analysis was employed for load application, as the simulated system was not time-dependent. The load was applied as a downward displacement across the top surface of the loading region. Two types of supports were used:

- Pin Support: Restrained both vertical and longitudinal displacements.
- Roller Support: Restrained only vertical displacements

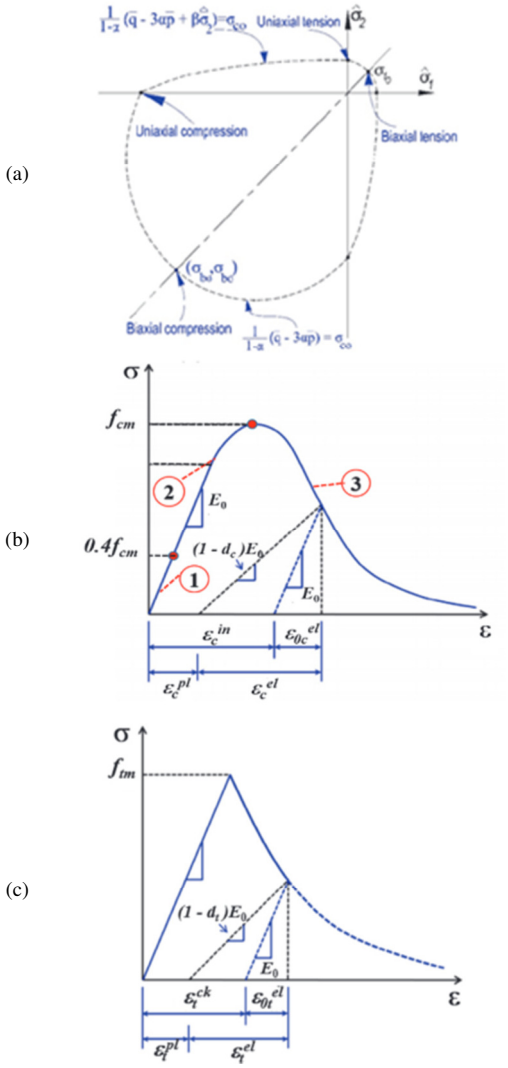

Fig. 11. Stress versus strain curve: (a) concrete yield surface, (b) behavior in compression, (c) behavior in tension.

V. VERIFICATION RESULTS OF FEM

The FEA results were compiled and compared with experimental data to validate the numerical model. The comparison focused on the ultimate load capacity, crack pattern and failure mechanisms, and ultimate deflection. The FEA demonstrated excellent agreement with the experimental results, accurately replicating the slab load-carrying capacity and deflection behavior under various reinforcement ratios and strengthening techniques using steel boxes. The load-displacement curves from the FEA closely matched the experimental data, reflecting the same trends and behaviors observed during testing. The maximum load-carrying capacity and corresponding displacements for both experimental and numerical results are shown in Figure 12. The numerical model exhibited a maximum variance of about 8% for specimens with higher reinforcement ratios and approximately 5% for those with lower reinforcement ratios, confirming the reliability of the finite element approach. Detailed comparisons are summarized in Table VII, further highlighting the effectiveness of the numerical model in predicting the structural performance of GFRP-RC slabs.

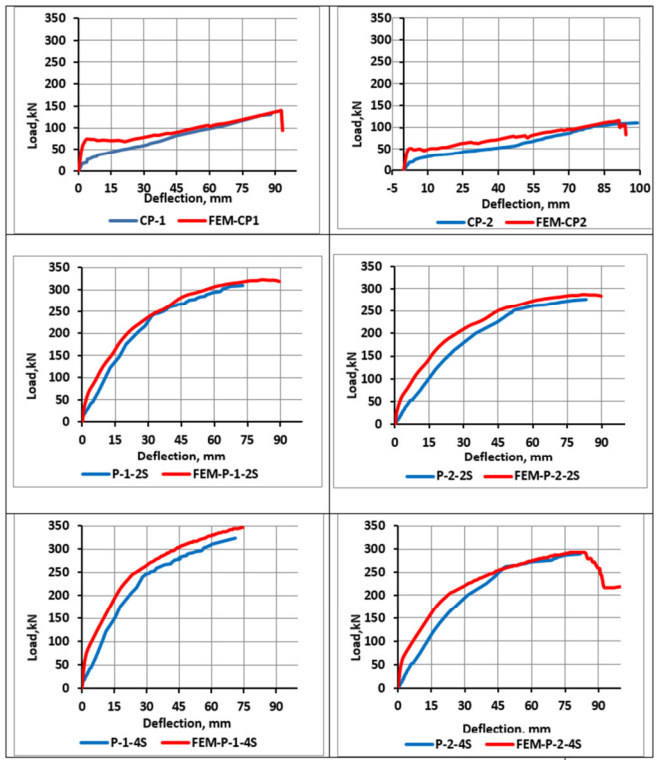

Fig. 12. The load deflection curve of the numerical and experimental simulation.

TABLE VII. COMPARISON BETWEEN THE NUMERICAL AND THE EXPERIMENTAL ULTIMATE LOAD

Specimens	P_u (FEA)	P_u (Exp.)	Ultimate Load Ratio
CP1	140	130	1.08
P-1-2S	321	310	1.04
P-1-4S	344	323	1.07
CP2	116	111	1.05
P-2-2S	286	276	1.04
P-2-4S	293	289	1.01

VI. CONCLUSION

This research focused on evaluating the flexural behavior of one-way concrete slabs reinforced with Glass Fiber-Reinforced Polymer (GFRP) bars and internally strengthened with

embedded steel sections. By applying static two-point bending tests, the study assessed critical flexural characteristics, such as cracking, deflection response, ultimate strength, and failure mechanisms. The following conclusions summarize the findings derived from experimental and numerical analyses:

- Slabs reinforced with GFRP bars demonstrated a bilinear response up to failure.
- The non-strengthened slab with a lower reinforcement ratio (CP-2) exhibited a reduction in ultimate strength compared to the solid slab (CP-1) with a higher reinforcement ratio, primarily due to reduced reinforcement. The strengthened specimens showed further variations in strength based on the reinforcement configuration.
- The internal steel strengthening improved the slabs' performance by mitigating cracks during the service stage, enhancing the stiffness, load-carrying capacity, flexural strength, and shear resistance, and increasing the first cracking load.
- The strengthened slabs exhibited significantly reduced deflection compared to the non-strengthened slabs.
- Strengthening significantly reduced the maximum crack width and number of cracks compared to the non-strengthened slabs.
- The non-strengthened slabs failed in a brittle flexural tension mode due to GFRP bar rupture (tension-controlled design). In contrast, the strengthened slabs failed in a brittle flexural compression mode due to concrete crushing, with internal steel shapes shifting the failure zone from tension to compression.
- The slabs with a GFRP reinforcement ratio of 0.532% exhibited higher load-carrying capacity compared to those with a 0.266% reinforcement ratio.
- The slabs strengthened with four steel shapes outperformed those with two steel shapes, demonstrating reduced deflection and cracking alongside improved ultimate capacity, stiffness, and flexural strength.
- The Finite element analysis using the Abaqus software showed excellent agreement with the experimental results, validating the model's accuracy in predicting the load-deflection behavior, crack patterns, and failure mechanisms.

This study confirms that the integration of GFRP bars with internal steel strengthening significantly enhances the structural performance of concrete slabs, providing insights for designing robust and efficient structural systems.

REFERENCES

[1] S. Wang, J. Tang, Y. Zou, and Q. Zhou, "Research on production process optimization of precast concrete component factory based on value stream mapping," *Engineering, Construction and Architectural Management*, vol. 27, no. 4, pp. 850–871, Nov. 2019, https://doi.org/10.1108/ECAM-10-2018-0455.

[2] J. Bai, *Advanced Fibre-Reinforced Polymer (FRP) Composites for Structural Applications*, 2nd ed. Sawston, Cambridge, UK: Woodhead Publishing, 2022.

[3] J. Qureshi, "A Review of Fiber Reinforced Polymer Structures," *Fibers*, vol. 10, no. 3, Mar. 2022, Art. no. 27, https://doi.org/10.3390/fib10030027.

[4] M. Abdulkhaliq and A. H. Al-Ahmed, "The Flexural Behavior of One-Way Concrete Bubbled Slabs Reinforced by GFRP-Bars with Embedded Steel I-Sections," *Engineering, Technology & Applied Science Research*, vol. 14, no. 4, pp. 15860–15870, Aug. 2024, https://doi.org/10.48084/etasr.7680.

[5] S. Waghmare, S. Shelare, K. Aglawe, and P. Khope, "A mini review on fibre reinforced polymer composites,", *Materials Today: Proceedings*, Jan. 2022, vol. 54, pp. 682–689, https://doi.org/10.1016/j.matpr.2021.10.379.

[6] S. Reichenbach, P. Preinstorfer, M. Hammerl, and B. Kromoser, "A review on embedded fibre-reinforced polymer reinforcement in structural concrete in Europe," *Construction and Building Materials*, vol. 307, Nov. 2021, Art. no. 124946, https://doi.org/10.1016/j.conbuildmat.2021.124946.

[7] M. Abdulkhaliq and A. H. Al-Ahmed, "Behavior of GFRP Reinforced-Concrete Bubbled One-Way Slabs by Encased Composite Steel I-Sections," *Engineering, Technology & Applied Science Research*, vol. 14, no. 5, pp. 16701–16712, Oct. 2024, https://doi.org/10.48084/etasr.8123.

[8] A. Jalil and A. H. Al-Zuhairi, "Behavior of post-tensioned concrete girders subject to partially strand damage and strengthened by NSM-CFRP composites," *Civil Engineering Journal*, vol. 8, no. 7, pp. 1507–1521, 2022.

[9] M. R. Khalaf, A. H. A. Al-Ahmed, A. A. Allawi, and A. El-Zohairy, "Strengthening of Continuous Reinforced Concrete Deep Beams with Large Openings Using CFRP Strips," *Materials*, vol. 14, no. 11, Jan. 2021, Art. no. 3119, https://doi.org/10.3390/ma14113119.

[10] A. Q. Mohammad and R. M. Abbas, "Structural Behavior of Prestressed RC Dapped Beam with Openings Strengthened Using CFRP Sheets," in *International Conference on Geotechnical Engineering and Energetic*, Iraq, 2023, Art. no. 02004, https://doi.org/10.1051/e3sconf/202342702004.

[11] S. Sirimontree, S. Keawsawasvong, and C. Thongchom, "Flexural Behavior of Concrete Beam Reinforced with GFRP Bars Compared to Concrete Beam Reinforced with Conventional Steel Reinforcements," *Journal of Applied Science and Engineering*, vol. 24, no. 6, pp. 883–890, 2021, https://doi.org/10.6180/jase.202112_24(6).0009.

[12] S. A. Jabbar and S. B. H. Farid, "Replacement of steel rebars by GFRP rebars in the concrete structures," *Karbala International Journal of Modern Science*, vol. 4, no. 2, pp. 216–227, Jun. 2018, https://doi.org/10.1016/j.kijoms.2018.02.002.

[13] S. A. Sheikh and Z. Kharal, "Replacement of steel with GFRP for sustainable reinforced concrete," *Construction and Building Materials*, vol. 160, pp. 767–774, Jan. 2018, https://doi.org/10.1016/j.conbuildmat.2017.12.141.

[14] P. Qiao, Q. Liu, Z. Lu, and Z. Wang, "Flexural behaviour of GFRP-encased concrete panels," *Magazine of Concrete Research*, vol. 70, no. 24, pp. 1265–1279, Dec. 2018, https://doi.org/10.1680/jmacr.17.00423.

[15] T. Liu, P. Feng, X. Lu, J.-Q. Yang, and Y. Wu, "Flexural behavior of novel hybrid multicell GFRP-concrete beam," *Composite Structures*, vol. 250, Oct. 2020, Art. no. 112606, https://doi.org/10.1016/j.compstruct.2020.112606.

[16] J. Di, L. Cao, and J. Han, "Experimental Study on the Shear Behavior of GFRP–Concrete Composite Beam Connections," *Materials*, vol. 13, no. 5, Jan. 2020, Art. no. 1067, https://doi.org/10.3390/ma13051067.

[17] M. M. Hason, A. H. Al-Zuhairi, A. N. Hanoon, A. A. Abdulhameed, A. W. Al Zand, and I. S. Abbood, "Peak Ground Acceleration Models Predictions Utilizing Two Metaheuristic Optimization Techniques," *Latin American Journal of Solids and Structures*, vol. 19, Jun. 2022, Art. no. e447, https://doi.org/10.1590/1679-78256940.

[18] P. D. Gkournelos, T. C. Triantafillou, and D. A. Bournas, "Seismic upgrading of existing reinforced concrete buildings: A state-of-the-art review," *Engineering Structures*, vol. 240, Aug. 2021, Art. no. 112273, https://doi.org/10.1016/j.engstruct.2021.112273.

[19] G. de Matteis and M. Ferraioli, "Metal Shear Panels for Seismic Upgrading of RC Buildings: A Case Study," *Key Engineering Materials*, vol. 763, pp. 1058–1066, 2018, https://doi.org/10.4028/www.scientific.net/KEM.763.1058.

[20] P. Szewczyk, "Experimental and Numerical Study of Steel–Concrete Composite Beams Strengthened under Load," *Materials*, vol. 17, no. 18, 2024, Art. no. 4510.

[21] P. Matchan, S. Sirimontree, and B. Witchayagkoon, "Simulation of Flexural Behavior of Damaged Prestressed Concrete Beam by Finite Element Method," *International Transaction Journal of Engineering, Management, & Applied Sciences & Technologies*, vol. 6, no. 5, pp. 225–234, 2015.

[22] F. H. Ibrahim and A. H. Ali Al-Ahmed, "Finite Element Analysis of Cracked One-Way Bubbled Slabs Strengthened By External Prestressed Strands," *Journal of Engineering*, vol. 27, no. 1, pp. 46–66, Jan. 2021.

[23] M. Abramowicz, S. Berczyński, and T. Wróblewski, "Modelling and parameter identification of steel–concrete composite beams in 3D rigid finite element method," *Archives of Civil and Mechanical Engineering*, vol. 20, no. 4, Sep. 2020, Art. no. 103, https://doi.org/10.1007/s43452-020-00100-7.

[24] Z. K. Al-Mamory and A. H. A. Al-Ahmed, "Behavior of steel fiber reinforced concrete beams with CFRP wrapped lap splice bars," *Structures*, vol. 44, pp. 1995–2011, Oct. 2022, https://doi.org/10.1016/j.istruc.2022.08.096.

[25] Y.-C. Ou, M.-S. Tsai, K.-Y. Liu, and K.-C. Chang, "Compressive Behavior of Steel-Fiber-Reinforced Concrete with a High Reinforcing Index," *Journal of Materials in Civil Engineering*, vol. 24, no. 2, pp. 207–215, Feb. 2012, https://doi.org/10.1061/(ASCE)MT.1943-5533.0000372.

[26] A. Mathern and J. Yang, "A Practical Finite Element Modeling Strategy to Capture Cracking and Crushing Behavior of Reinforced Concrete Structures," *Materials*, vol. 14, no. 3, Jan. 2021, Art. no. 506, https://doi.org/10.3390/ma14030506.

[27] S. A. Mohammed and A. I. Said, "Analysis of concrete beams reinforced by GFRP bars with varying parameters," *Journal of the Mechanical Behavior of Materials*, vol. 31, no. 1, pp. 767–774, Jan. 2022, https://doi.org/10.1515/jmbm-2022-0068.

[28] A. Raza, Q. uz Z. Khan, and A. Ahmad, "Numerical Investigation of Load-Carrying Capacity of GFRP-Reinforced Rectangular Concrete Members Using CDP Model in ABAQUS," *Advances in Civil Engineering*, vol. 2019, no. 1, 2019, Art. no. 1745341, https://doi.org/10.1155/2019/1745341.

[29] P. Zhang *et al.*, "Influence factors analysis of the interfacial bond behavior between GFRP plates, concrete," *Structures*, vol. 26, pp. 79–91, Aug. 2020, https://doi.org/10.1016/j.istruc.2020.04.005.

[30] A. Hussein Ali Al-Ahmed, A. Al-Rumaithi, A. A. Allawi, and A. El-Zohairy, "Mesoscale analysis of Fiber-Reinforced concrete beams," *Engineering Structures*, vol. 266, Sep. 2022, Art. no. 114575, https://doi.org/10.1016/j.engstruct.2022.114575.